BIOCHEMISTRY

Article

The PT1#Ca Gla Domain Binds to a Membrane through Two Dipalmitoylphosphatidylserines. A Computational Study

Yoel Rodri#guez, Mihaly Mezei, and Roman Osman

Biochemistry, **2008**, 47 (50), 13267-13278 • Publication Date (Web): 17 November 2008

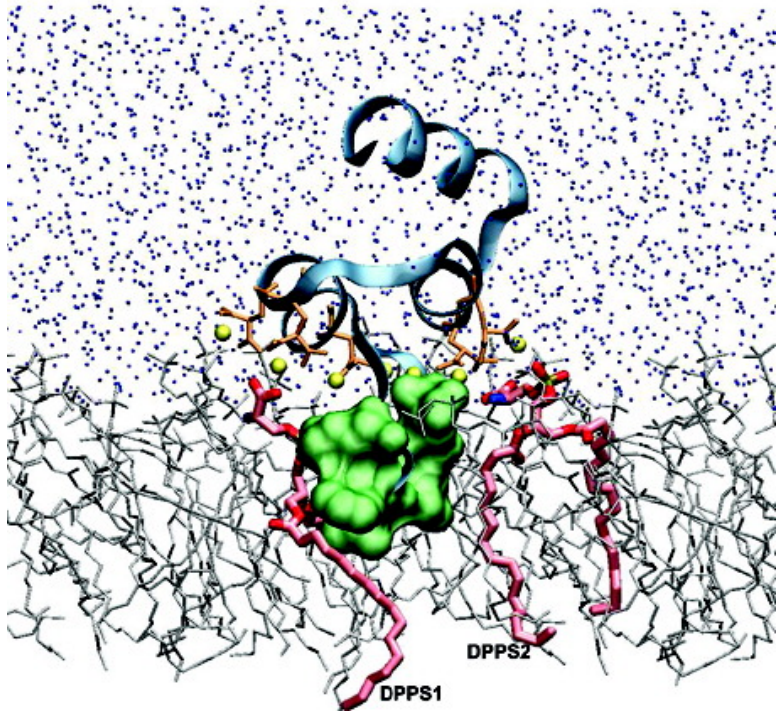

More About This Article

Additional resources and features associated with this article are available within the HTML version:

- Supporting Information
- Access to high resolution figures
- Links to articles and content related to this article
- Copyright permission to reproduce figures and/or text from this article

Biochemistry is published by the American Chemical Society. 1155 Sixteenth Street N.W., Washington, DC 20036

The PT1−Ca^{2+} Gla Domain Binds to a Membrane through Two Dipalmitoylphosphatidylserines. A Computational Study†

Yoel Rodríguez,‡,§ Mihaly Mezei,‡ and Roman Osman*,‡

Department of Structural and Chemical Biology, Mount Sinai School of Medicine, New York, New York 10029, and CUNY Natural Sciences Department, Hostos Community College, Bronx, New York 10451

Received June 26, 2008; Revised Manuscript Received September 17, 2008

ABSTRACT: Binding of vitamin K-dependent proteins to cell membranes containing phosphatidylserine (PS) via γ-carboxyglutamic acid (Gla) domains is one of the essential steps in the blood coagulation pathway. During activation of the coagulation cascade, prothrombin is converted to thrombin by prothrombinase, a complex consisting of serine protease FXa and cofactor FVa, anchored to anionic phospholipids on the surface of activated platelets in the presence of calcium ions. To investigate the binding of the Gla domain of prothrombin fragment 1 (PT1) to anionic lipids in the presence of Ca^{2+}, we have conducted MD simulations of the protein with one and two dipalmitoylphosphatidylserines (DPPS) in a dipalmitoylphosphatidylcholine (DPPC) bilayer membrane. The results show a well-defined phosphatidylserine binding site, which agrees generally with crystallographic studies [Huang, M., et al. (2003) *Nat. Struct. Biol. 10*, 751−756]. However, in the presence of the lipid membrane, some of the interactions observed in the crystal structure adjust during the simulations possibly because in our system the PT1−Ca^{2+} complex is embedded in a DPPC lipid membrane. Our simulations confirm the existence of a second phospholipid headgroup binding site on the opposite face of the PT1−Ca^{2+} complex as suggested by MacDonald et al. [(1997) *Biochemistry 36*, 5120−5127]. The serine headgroup in the second site binds through a Gla domain-bound calcium ion Ca1, Gla30, and Lys11. On the basis of free energy simulations, we estimate the energy of binding of the PT1−Ca^{2+} complex to a single DPPS to be around −11.5 kcal/mol. The estimated free energy of binding of a DPPS lipid to the second binding site is around −8.8 kcal/mol and is in part caused by the nature of the second site and in part by entropic effects.

Protein−membrane and lipid−lipid interactions play an important role in the blood coagulation pathway as well as in many other physiological processes. In the blood coagulation pathway, vascular tissue damage exposes negatively charged phospholipids such as phosphatidylserines (PSs)[1] on the surface of epithelial cells. In a Ca^{2+}-dependent process, the blood-borne proteases are anchored to the negatively charged phospholipids through the N-terminal domains that contain γ-carboxyglutamic acids (Gla) (*1, 2*). Inhibition of the vitamin K-dependent post-translational modification of glutamates to Gla is a widely used anticoagulant therapy (*3*). It has been shown that the binding of vitamin K-dependent clotting factors and their cofactors to the lipid surface via the Gla domains enhances the catalytic efficiency of the clotting reactions (*4*). The Gla domains form the basis of a mechanism for protein−phospholipid membrane interaction (*5*). Frequently, these domains interact with negatively charged membranes. However, because the modified Gla residues are negatively charged, their interaction with the lipids is mediated via positively charged ions, usually, Ca^{2+}. In addition to their essential role in blood coagulation proteins, the Gla domains are also present in other proteins such as osteocalcin, matrix Gla protein, and transmembrane Gla proteins 3 and 4 (*6*). The first two proteins are required for regulation of bone growth and extraosseous calcification (*7*). A very common negatively charged lipid is PS, which has been shown to anchor the Gla domain of prothrombin through interaction via Ca^{2+} ions (*5*). PSs have also been shown to bind to regulatory sites other than Gla domains, e.g., on zymogene II, factor Xa, and cofactor Va (*8*). PSs regulate allosterically both factor Xa and factor Va (*8*−*10*). Finally, PSs in the platelet membrane have been proposed to act as second messengers because they link platelet activation to thrombin generation (*2*).

Unlike many globular protein domains in which hydrophobic packing within the core of the protein domain stabilizes the structure, the tertiary fold of the Gla domain is stabilized by a linear array of internal Ca^{2+} ions bound to the Gla side chain carboxyl groups (*11, 12*). Calcium ion binding to the Gla domain induces a marked structural

† Part of this work was supported by Ministerio de Educación y Ciencia of Spain through a postdoctoral fellowship to Y.R.

* To whom correspondence should be addressed. E-mail: Roman.Osman@mssm.edu. Telephone: (212) 659-8627. Fax: (212) 849-2456.

‡ Mount Sinai School of Medicine.

§ Hostos Community College.

[1] Abbreviations: Gla, γ-carboxyglutamic acid; DPPS, dipalmitoylphosphatidylserine; DPPC, dipalmitoylphosphatidylcholine; PS, phosphatidylserine; PC, phosphatidylcholine; PT1, prothrombin fragment 1; Ca^{2+}, calcium ion; PDB, Protein Data Bank; MD, molecular dynamics; CPTA, constant pressure, temperature, and area protocol; rmsd, root-mean-square deviation; FEP, free energy perturbation; TI, thermodynamic integration.

10.1021/bi801199v CCC: $40.75
Published on Web 11/17/2008

transition from a largely unfolded and nonfunctional domain to one that is tightly folded and able to bind to membranes. A hydrophobic patch in the N-terminus of Gla domains (e.g., Phe5, Leu6, and Val9 in bovine prothrombin) forms part of the ω-loop region, which plays an important role in phospholipid membrane binding (*13*). Recently, the structural basis of PS specificity for Gla domains has been elucidated in a crystal structure of bovine PT1, in a complex with Ca^{2+} ions and lysophosphatidylserine (lysoPS) (*5*). In that structure, the serine headgroup interacts with the Gla domain through a Ca^{2+} ion and Gla residues 17 and 21, which are highly conserved in the Gla domain fold. A similar site that forms another surface cavity surrounded by Gla30, Gla8, and Lys11 has been proposed as a potential binding site for another PS (*14*). In spite of the fact that it shows all the characteristics of a PS binding site, this site remains unoccupied in the crystal structure. Thus, the question whether the observed cavity is a PS binding site remains unresolved.

Despite homology in the sequence and structure of vitamin K-dependent proteins, they show a striking variety in membrane binding properties (*14*). The biological role of such diversity may be related to simultaneous association of proteins with membranes and other proteins. McDonald et al. (*14*) characterized the membrane binding properties of human and bovine forms of vitamin K-dependent proteins Z, S, and C, which show unique properties and interspecies differences that correlate with specific amino acid sequence variations in the amino terminus. Bovine protein Z exhibits higher membrane binding affinities than human protein Z, which correlates with the substitution of Asp in position 34 with Asn. The same kind of correlated substitution was found in human and bovine protein S, where Asp in position 35 corresponds to the protein with the higher affinity. Factor X, a high-affinity protein, also contains an Asp at position 34. Residues in position 11 seem to play a key role in membrane binding. Protein Z shows 100-fold slower binding kinetics relative to other vitamin K-dependent proteins, a fact which seems to be related to the unique placement of Gla at position 11. Protein C displays 100−1000-fold lower binding affinities than the other proteins, which may be due to a Pro at position 11 (bovine protein C). This is shared with factor VII, also of the low-affinity protein. Loss of Gla32 (Gln32) (homologous to Gla33 of protein Z) appears to be related to low affinity in protein C as well. Factor VII, which contains substitutions at both positions (11 and 33) exhibits the lowest membrane affinity. The coordinated binding of two components to a membrane will increase the affinity of the complex. This in turn can limit exchange of the protein from the membrane and may become the rate-limiting process in an enzymatic reaction such as in the catalytic action of prothrombinase (*14*). In an analogous manner, a second phosphatidylserine binding site in PT1−Ca^{2+} protein could increase its affinity for the membrane and limit its exchange from the membrane. The elucidation of the mechanism by which the diversity of affinity is created through additional membrane contact sites will help our understanding of the structural role of γ-carboxyglutamic acids.

Using the available crystal structure of the binary PT1−Ca^{2+} complex and the ternary PT1−Ca^{2+}−lysoPS complex (*5*) (PDB entry 1NL2), we have constructed a model system in which PT1 is bound to a mixed bilayer membrane containing phosphatidylcholine (PC) and PS lipids. The aim of this work is to investigate the molecular basis of Gla domain binding specificity for phosphatidylserine-containing membranes. We present the results of free energy perturbation (FEP) and molecular dynamics (MD) simulations of the PT1−Ca^{2+}(1−46) complex binding to a pure PC membrane compared to the mixed membrane that contains PS. We analyze the contributions of the Gla residues, as well as other residues in the PS binding pockets, to the specificity for phosphatidylserine. An examination of the membrane-bound PT1 reveals the existence of a potential second binding site for PS, in agreement with the previous proposal (*14*). Simulations in the presence of another PS show the origin of the essential energetic difference between the two binding sites.

Table 1: Systems Simulated

system	constituents	representation
1	1 DPPS, 47 DPPCs, 3924 waters, 1 Na^+	(**1PS**)$_{PC}$
2	1 DPPS, 44 DPPCs, PT1−Ca^{2+}, 3680 waters, 2 Na^+	(PT1−Ca^{2+}/**1PS**)$_{PC}$
3	2 DPPSs, 43 DPPCs, PT1−Ca^{2+}, 3679 waters, 3 Na^+	(PT1−Ca^{2+}/**2PS**)$_{PC}$

METHODS AND MODELS

Membrane Model. The construction of the lipid membrane followed a standard protocol (*15*). The general strategy is to randomly select phospholipids from a pre-equilibrated and prehydrated library of dipalmitoylphosphatidylcholine (DPPC) generated by Monte Carlo simulations in the presence of a mean field (*16*−*18*). The lipids are placed in a periodic system, and the number of overlaps between heavy atoms is reduced through systematic rotations around the Z axis and translations in the $X-Y$ plane. All waters that overlap with the hydrocarbon interior of the bilayer, between $\pm$12 Å in the Z direction, were deleted. Three different systems were built: (1) a mixed bilayer membrane composed of one DPPS in 47 DPPCs without protein [(**1PS**)$_{PC}$], (2) the PT1−Ca^{2+}(1−46) complex (PDB entry 1NL2) bound to a mixed bilayer membrane containing one PS in a PC membrane [(PT1−Ca^{2+}/**1PS**)$_{PC}$], and (3) PT1−Ca^{2+}(1−46) complex bound to a mixed bilayer membrane containing two PSs in a PC membrane [(PT1−Ca^{2+}/**2PS**)$_{PC}$]. The first model included 47 DPPCs, one DPPS, and 3924 water molecules. A Na^+ was added for charge neutrality of the simulation cell. The second system comprised of the PT1−Ca^{2+}(1−46 residues,7Ca^{2+}) complex, 44 DPPCs, one DPPS, and 3680 water molecules was neutralized with two Na^+ ions. The third system was formed by the PT1−Ca^{2+} complex, two DPPSs, 43 DPPCs, and 3679 water molecules and neutralized via addition of three Na^+ ions (see Table 1).

Setup of the Simulations. To construct the first system [(**1PS**)$_{PC}$], a pre-equilibrated pure DPPC membrane (5 ns of MD simulation) was used (*19*). For this pre-equilibrated pure membrane, hexagonal periodic boundary conditions were applied in the $X-Y$ plane to maximize the distance between two periodic images (*20*). The edge of the hexagon and the length of the prism were ~23.7 and ~120.0 Å, respectively, with a center-to-center distance between neighboring cell centers of ~41.0 Å, and the center of the bilayer membrane

was located at the *Z* origin. The all-atom CHARMM27 force field for phospholipids (*21*) and the TIP3P water model (*22*) were used in all calculations. Long-range interactions were treated by a group-based spherical cutoff at 14 Å. The van der Waals and electrostatic interactions were smoothly switched off at around a cutoff distance of 9.0 Å. The equilibration was carried out using Langevin dynamics with decreasing planar harmonic constraints of 10, 5, 1, 0.5, and 0 kcal mol^{-1} $Å^2$ on water, lipids, and protein (second system) for 25 ps in each stage, so that by the end of 125 ps, the entire system was completely unrestrained. This was followed with a constant pressure, temperature, and area protocol (CPTA) production MD for 5 ns. The temperature of the system was maintained at 330 K, which is above the gel−liquid crystal phase transition of DPPC. In the production stage, the temperature was maintained using the Nose-Hoover scheme. The length of all bonds involving hydrogen atoms was kept fixed with the SHAKE algorithm (*23*). The equations of motion were integrated with a time step of 2 fs. Then, one DPPC was replaced with one DPPS, and the system was shortly minimized, followed by heating to 330 K over 30 ps. A production MD simulation was performed for 1 ns using the NPT ensemble. The molecular dynamics and free energy simulations (see Free Energy Simulation Methods) were performed using CHARMM (*24*).

In the construction of the second system, the calculated cross-sectional area of the PT1−Ca^{2+} complex (∼180 $Å^2$) was equivalent to that of three DPPCs, which were replaced by the protein. The protein was placed in one leaflet of the phospholipid bilayer with the Phe5 residue from the ω-loop at a penetration depth of ∼7 Å in the membrane (*13*), based on a bilayer thickness of ∼38 Å. A longer MD simulation of the second system, (PT1−Ca^{2+}/**1PS**)$_{PC}$, was performed using NAMD (*25*). The system was initially subjected to a short minimization, followed by heating to 330 K over 30 ps. Twin-range nonbonded cutoffs of 10 and 12 Å were used for the Lennard-Jones potentials, and electrostatic interactions were calculated using particle-mesh Ewald summation (*26, 27*). The equilibration and the production MD simulations were carried out for 20 ns using the NPT ensemble.

Free Energy Simulation Methods. A conventional approach to the evaluation of the free energy of association in fluid mixtures relies on the calculation of the free energy profile of the selected species as a function of the distance that separates them. For lipid bilayers, such a calculation presents formidable difficulties due to the extremely slow lateral diffusion of lipid molecules (*19*). We therefore decided to perform simultaneous exchanges of lipid headgroups in the presence of the protein from a (PT1−Ca^{2+}/**PS**)$_{PC}$ configuration into a (PT1−Ca^{2+}/**PC**)$_{PC}$ configuration and vice versa on the basis of our previous success in evaluating the free energy of PS association in a mixed membrane of DPPC (*19*). The same exchange was done in the absence of the protein. In addition to eliminating the calculation of a distance-dependent free energy profile, this approach has an advantage in that the mutations involve only the headgroups since the hydrocarbon chains of DPPC and DPPS are identical. Because the lipid portions of PC and PS are the same, we used a dual topology of the PS−PC hybrid that involves only the headgroups (see Figure 1 in ref *19* and Figure S1 of the Supporting Information). In this approach, the parts of the system that are different in the initial and final states coexist at all times as the free energy simulation is carried out. They interact with the environment but not with each other (*28*). Thus, in the potential energy of this system, expressed as a function of a parameter λ that describes such a transformation, only the phosphocholine of the PC and phosphoserine of the PS are weighted by λ:

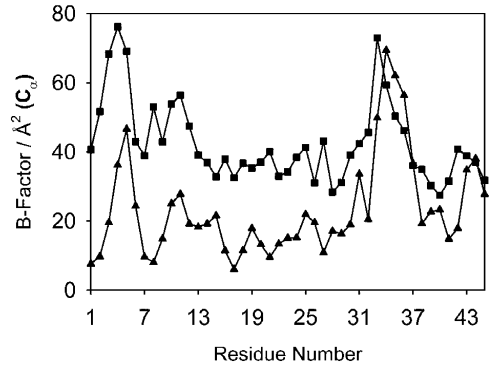

FIGURE 1: Debye−Waller *B* factors for the PT1 residues (1−46): experimental (■) and theoretical (▲) values.

$$U(\mathbf{r},\lambda) = U_0(\mathbf{r}) + \lambda U_b(r) + (1-\lambda)U_a(\mathbf{r}) \quad a = (PS^F, PC^B),\ b = (PC^F, PS^B) \quad (1)$$

The free energy calculations were performed in the forward (PS → PC^F) and backward (PC → PS^B) directions, in the presence (bound system) and absence (unbound system) of the protein (PT1−Ca^{2+}). The potential energy of each system is expressed in eq 1 with the directions represented by the superscripts (i.e., F and B mean forward and backward directions, respectively). $U_{PS}(\mathbf{r})$, $U_{PC}(\mathbf{r})$, and $U_0(\mathbf{r})$ are the contributions of PS, PC, and the rest of the system, respectively (*29, 30*). Phosphates of the two lipids as well as the first carbon of the glycerol with its hydrogens are included in the dual topology because they belong to the same group and have different partial charges in the CHARMM force field (*21*) (see Figure 1 of ref *19* and Figure S1 of the Supporting Information).

The ideal gas molecule end states for the dual topology simulation, one of the recent developments in the free energy methodology, were used in this study. Only the nonbonded interactions are scaled during the free energy simulation; the bonded terms are not scaled. This approach has shown good results in the case of the calculation of the double free energy difference ($\Delta\Delta G^{Binding}$) (*31, 32*).

The free energy simulations at different λ values were performed using the BLOCK module in CHARMM (*19, 33, 34*). Three blocks were defined: one for the reactant, one for the product, and one for the rest of the system. Blocks 2 and 3 consisted of the choline and phosphate groups of PC and serine and phosphate groups of PS, respectively, as described previously (*19*). The rest of the system formed block 1. The interaction energy between block 2 and block 3 was set to zero to eliminate unphysical interaction terms.

Both the free energy perturbation (FEP) and the thermodynamic integration (TI) methods were used to compute the free energy for each λ window on the same runs. The free energy difference using FEP was computed with the following equation:

$$\Delta G^{PS\rightarrow PC^F}_{PC\rightarrow PS^B} = -k_B T \sum_{i=1}^{n} \ln\left\langle e^{-[U^{F(B)}(\mathbf{r};\lambda_{i+1}) - U^{F(B)}(\mathbf{r};\lambda_i)]/k_B T}\right\rangle_{\lambda_i} \quad (2)$$

Scheme 1: Thermodynamic Cycle[a]

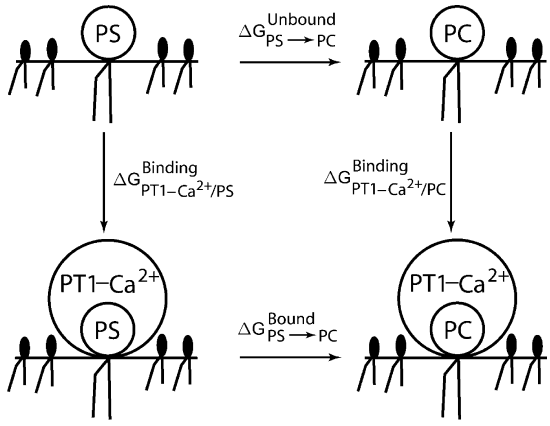

[a] The alchemical transformations are represented with horizontal arrows, $\Delta G_{PS\rightarrow PC}^{Bound}$ and $\Delta G_{PS\rightarrow PC}^{Unbound}$, and the physical transformations with vertical arrows, $\Delta G_{PT1-Ca^{2+}}^{Binding}$/PS and $\Delta G_{PT1-Ca^{2+}}^{Binding}$/PC.

where the angle brackets with the subscript λ_i indicate averaging over the simulation at λ_i and the sum is over n windows. In our calculations, double-wide sampling was used so that the perturbation was to the halfway point between the λ values. The free energy difference of the interconversion between PS/PC and PC/PS mixtures is given by $\Delta G_{PS\rightarrow PC^F}$ and $\Delta G_{PC\rightarrow PS^B}$, respectively. The superscripts on the potential energy, $U^{F(B)}(\mathbf{r};\lambda_{i+1})$ and $U^{F(B)}(\mathbf{r};\lambda_i)$, refer to the specific interconversion (i.e., forward or backward direction).

When TI is used, the total free energy difference between $\lambda = 0$ and $\lambda = 1$ for a linear λ dependence is

$$\Delta G_{PC\rightarrow PS^B}^{PS\rightarrow PC^F} = \int_{\lambda=0}^{\lambda=1} \langle U_b(\mathbf{r}) - U_a(\mathbf{r})\rangle_\lambda \, d\lambda \quad (3)$$

Both methods have been shown to reproduce experimental values of the free energy differences in several systems (e.g., refs *35*−*37*).

Free Energy Simulations. To obtain the free energy of binding of the PT1−Ca^{2+} complex to the mixed membrane that contains PS and PC relative to the membrane that contains only PC, a thermodynamic cycle was designed (Scheme 1). We performed FEP/TI simulations to obtain the free energy difference [$\Delta G_{PS\rightarrow PC^F}^{Bound}$(PC→$PS^B$)] of the alchemical transformation of (PT1−Ca^{2+}/**PS^F**(**PC^B**))$_{PC}$ to (PT1−Ca^{2+}/**PC^F**(**PS^B**))$_{PC}$ with the lipid headgroup bound to the face of the Gla domain as in Huang et al. (*5*). Likewise, in the absence of the PT1−Ca^{2+} complex, the free energy difference [$\Delta G_{PS\rightarrow PC^F}^{Unbound}$(PC→$PS^B$)] of the same alchemical transformation was determined. The alchemical changes in the absence and presence of the PT1−Ca^{2+} complex yield a value that should equal the energy difference of PT1 interacting with a pure PC membrane or with a membrane that contains a PS. The free energy of binding of the PT1−Ca^{2+} complex to the mixed membrane that contains PS and PC relative to a membrane that contains only PC is represented by the following relationship (see Scheme 1):

$$\Delta\Delta G^{Binding} = \Delta G_{PT1-Ca^{2+}/PC^F,PT1-Ca^{2+}/PS^B}^{Binding} - \Delta G_{PT1-Ca^{2+}/PS^F,PT1-Ca^{2+}/PC^B}^{Binding} = \Delta G_{PS\rightarrow PC^F(PC\rightarrow PS^B)}^{Bound} - \Delta G_{PS\rightarrow PC^F(PC\rightarrow PS^B)}^{Unbound} \quad (4)$$

Similar simulations were performed on the system in which another PS was bound to the other potential phosphatidylserine binding site (*14*).

Four different free energy simulations were performed for each binding site. Two of them correspond to the bound system [$\Delta G_{PS\rightarrow PC^F}^{Bound}$(PC→$PS^B$)] and the other two to the unbound system [$\Delta G_{PS\rightarrow PC^F}^{Unbound}$(PC→$PS^B$)].

Eleven λ windows (λ = 0.02, 0.1−0.9, and 0.98) were used to calculate the free energy differences with the FEP and TI methods. The initial value of λ was 0.02, and it was incremented from 0.1 to 0.9 in steps of 0.1; the final value was 0.98. Initially, the system was heated to 330 K and equilibrated for 100 ps at λ = 0.02. At each λ value, the system was re-equilibrated for 50 ps, and data were collected for an additional 100 ps, during which the trajectory was recorded every 50 fs, producing 2000 frames for each λ value.

The trapezoidal rule was used to evaluate the integral from the discrete values of the free energy derivative between λ = 0.02 and λ = 0.98. To improve the evaluation of the integral (eq 3), three different schemes were applied to produce the end point contributions (regions near $\lambda = 0 \rightarrow 0.02$ and $\lambda = 0.98 \rightarrow 1$). A detailed explanation of the three schemes used to evaluate the integral in the TI can be found in ref *19*; all three schemes yield very similar results.

RESULTS AND DISCUSSION

Molecular Dynamics Simulations. The PT1−Ca^{2+} complex attached to the mixed membrane [(PT1−Ca^{2+}/**1PS**)$_{PC}$] was stable throughout the 20 ns of the MD simulation and exhibited a great degree of similarity to the known crystallographic structure. The root-mean-square deviation (rmsd) with respect to the crystal structure was 0.91 ± 0.09 Å (see Figure S2A of the Supporting Information). Since the crystal structure has a lysoPS group, we compared the position of the DPPS headgroup in the MD simulation to that in the crystal structure. Its rmsd with respect to the crystal structure was 0.85 ± 0.09 Å (see Figure S2B of the Supporting Information) in the last 12 ns of the simulation. To assess protein flexibility, the values of the Debye−Waller *B* factors were calculated using the well-known expression

$$B_i = (8\pi^2/3)\langle \mu_i^2 \rangle \quad (5)$$

where μ_i is the three-dimensional fluctuation of atom *i* around its mean position and angle brackets denote a time average over the course of the simulation. As seen in Figure 1, the simulation reproduces the flexibility of the α carbons in the crystal structure. The vertical shift observed between the simulation and the X-ray structure is due to the macroscopic lattice vibrations. Two regions of the PT1 protein show large fluctuations. One corresponds to the ω-loop that is involved in the interaction with the lipid; specifically, Phe5 and Leu6 exhibit the largest fluctuations around their mean positions even in the presence of the lipid. The other region is not involved in the phosphatidylserine binding pockets and forms a reverselike turn between two helices, Arg25−Ala31 and Ser36−Thr46.

Average Density Profile. The average density profile of the different components in both layers for the bound system in the last nanosecond of the simulation is depicted in Figure 2A. The number density of water outside the lipid is around

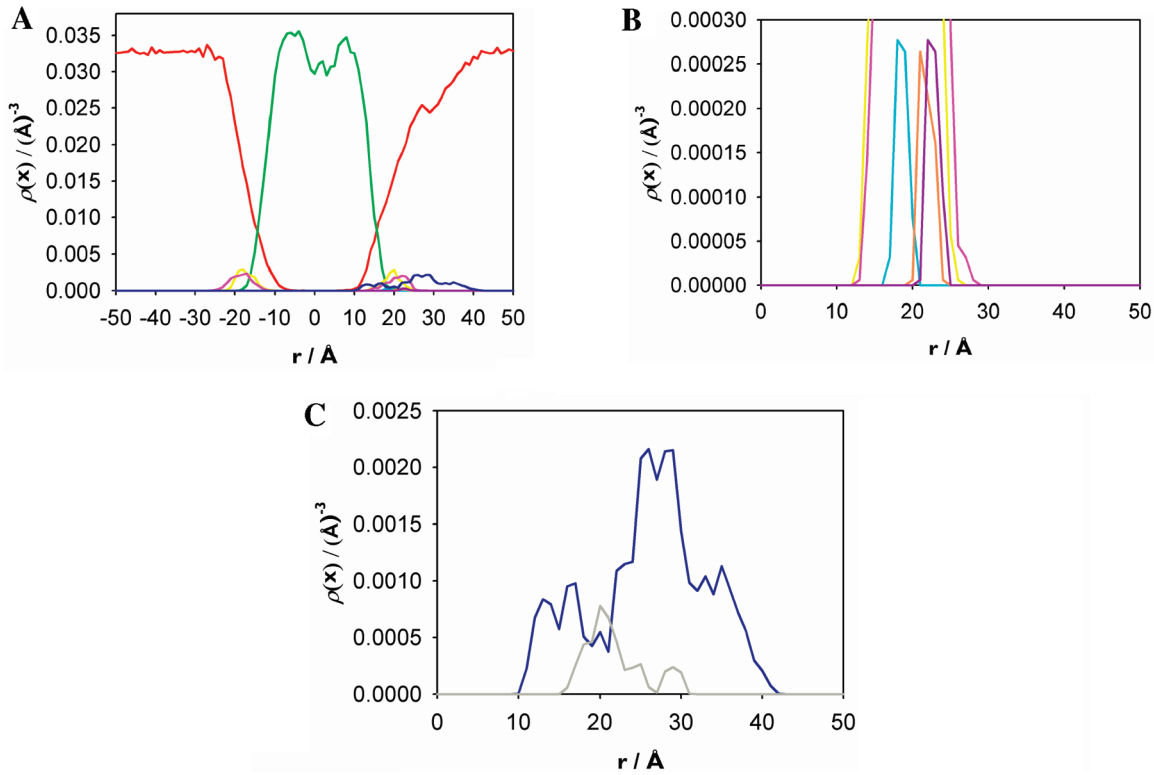

FIGURE 2: Density profile of the main components for the lipid membrane with the PT1−Ca^{2+} complex along the *Z* axis. The distributions of the waters (red), hydrocarbon chains (green), P (yellow) and N (pink) atoms of PC, P (cyan), N (orange), and carboxyl group atoms of PS (dark red), α carbons of PT1 protein (dark blue), and Ca^{2+} (gray) are shown. In panels B and C, the distributions of the components of PC and PS headgroups and PT1 and Ca^{2+} ions represented in panel A are magnified, respectively.

0.0333 Å^{-3}, as expected for a bulk solvent density, and it approaches zero in the hydrocarbon core region of the membrane. Clearly, on the side of the protein, both the density of the lipids and especially that of the water are substantially lower than on the opposite leaflet. The P and N atoms of the PC headgroup are located within the same region of the lipid, approximately 20 Å from the center of the membrane, reflecting the fact that the phosphorus−nitrogen vector ($\vec{}$PN) is approximately parallel to the membrane plane (Figure 2A). However, the angle between $\vec{}$PN and the outwardly directed bilayer normal, ∠PN$_N$, depends on the distance of the DPPCs from the protein. The ∠PN$_N$ is 52 ± 10° for DPPCs within ∼7 Å of the protein and 86 ± 13° for DPPCs beyond that distance. In contrast, the distributions of the P and N atoms of the PS headgroup span different regions (Figure 2B), with a tilt of 41 ± 5° between the headgroup dipole and the bilayer normal. This is most likely due to the interaction between the serine carboxyl group of PS and the Ca^{2+} ions in the Gla domain of PT1 on one hand and the interaction between the serine amino group and the phosphate oxygen of one DPPC on the other hand. The organization of the DPPC lipids proximal to the protein and their similar orientation with respect to the lipid allowed us to design the free energy perturbation simulations as described below. The density of the lipid hydrocarbon chain atoms is reduced near the center of the membrane, in agreement with other experiments and models of the bilayer system (*38*). The distribution of the calcium ions has mainly two peaks centered at 20 and 29 Å. The first distribution includes six Ca^{2+} ions, whereas Ca7 is farther from the lipid (Figure 2C). The C_α atoms of the PT1 protein span the region from 10 to 42 Å. The *ω*-loop is located between 10 and 17 Å, corresponding to the fact that the Phe5 residue from this

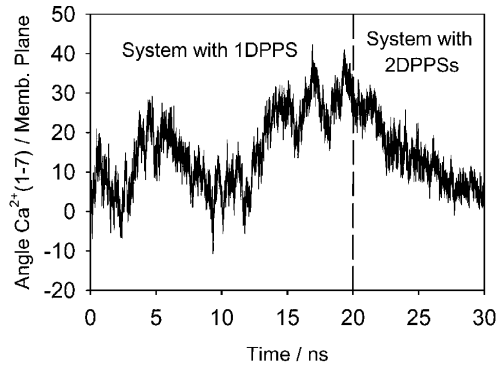

FIGURE 3: Angle of inclination of the PT1−Ca^{2+} complex with respect to the membrane lipid plane.

loop penetrates into the membrane at a depth of ∼7 Å (*13*) (Figure 2C). The density profiles of the water molecules, the hydrocarbon chain, and the P and N atoms of the PC and PS headgroups for the lipid membrane without the protein are similar to those in the layer without the protein (PT1−Ca^{2+}) of the bound system. The ∠PN$_N$ is 74 ± 22° for the DPPCs of the pure layer membrane, which is approximately the same as in our previous studies (*19*).

An interesting relation between the PT1−Ca^{2+} complex and the membrane seems to depend on the number of DPPS lipids that interact with it. The system in which the PT1−Ca^{2+} complex is bound to only one DPPS is characterized by an inclination of the proteins with respect to the lipid plane by ∼30°. The angle between the vector formed by two calcium atoms, Ca1 and Ca7, and the membrane plane, used to define such inclination, shows a progressive change from 0° to approximately 30° (Figure 3). Upon addition of the second DPPS, the protein approaches a parallel orienta-

Table 2: Root-Mean-Square Deviations between Average Simulated and Crystal Structures

	rmsd (only backbone) (Å)	rmsd (all atoms) (Å)
PT1−Ca^{2+}/**1PS**	0.82	3.44
PT1−Ca^{2+} (Ca^{2+})	0.73 (1.01)	1.69 (1.01)
ω-loop (residues 1−9)	0.89	1.65
DPPS	0.76[a]	4.49[a]

[a] Only N, Cα, carboxyl oxygen, and carbon atoms from the serine headgroup of DPPS were included in the rmsd calculation.

Table 3: Proximity Analysis Giving the Coordination Numbers of Ca5 and Ca6 before and after Serine Amino Group Shifts

	K coordination number (first shell radius of 3.2 Å)	
time (ns)	Ca5	Ca6
5.0	1.00	**1.83**
5.2	1.00	**1.75**
5.4	1.00	**1.75**
5.6	**1.22**	1.48
5.8	**1.34**	1.34
6.0	**1.41**	1.25
7.0	**1.78**	0.93
10.0	**1.82**	0.88
15.0	**1.88**	0.92
20.0	**1.86**	0.97

tion with respect to the membrane normal as indicated by the extended trajectory from 20 to 30 ns (Figure 3). Thus, if the orientation of the rest of the system attached to PT1 is important to its biological function (e.g., its interaction with prothrombinase), binding to the lipid through interaction with two DPPSs may provide a potentially important regulatory mechanism.

Phosphatidylserine Binding to the Gla Domain: First Binding Site. In the crystal structure of Huang et al. (*5*), the headgroup of the lysoPS is anchored to PT1 through an interaction with the protein-bound Ca^{2+} ions. We find that most of the interactions observed in the crystal (*5*) are maintained in our simulations. However, the results from the MD simulation indicate that the serine headgroup shifts from interacting with Ca5 and Ca6 to an interaction with only Ca6. Approximately 5.4 ns into the simulation, the distance between OT2 of serine and Ca6 shifts from 3.6 to 2.1 Å, providing a much stronger electrostatic interaction. At the same time, the OT1−Ca5 distance increases to >6 Å (see Figure 3SA of the Supporting Information). The available space around Ca5 is filled with water molecules that occupy its coordination sphere. A proximity analysis (*39*) at selected times (Table 3) shows that after the 5.4 ns point the solvation shells of Ca5 and Ca6 begin to rearrange. The rearrangement takes approximately 1.5 ns which can be seen from the rise in the number of water molecules around Ca5 and a parallel reduction in the coordination number around Ca6. At the end of the rearrangement, the coordination of Ca6 consists of the carboxyl oxygens of Gla20 (OE2) and Gla21 (OE2 and OE4), carboxyl oxygens (OT1 and OT2) of DPPS, and one water molecule. Ca5 is coordinated by the carboxyl oxygens of Gla7 (OE1 and OE2), Gla17 (OE3 and OE4), and Gla21 (OE1 and OE2) (not shown). Ca5 and Ca6 also interact with the backbone carbonyl oxygens of Ala1 and Arg16, respectively. Likewise, the serine carboxyl oxygens of DPPS interact with carboxyl oxygens of Gla17 (OE4) through water as well (Figure 4).

The terminal phosphate oxygens of DPPS, OP3 and OP4, bind to a positively charged patch formed by the NH1 group of Arg10 and the Nζ atom of Lys3. In the crystal structure, Arg16 has been identified as another member of the positive patch (see Figure 3SB of the Supporting Information). However, during the simulation, this residue shifts to interact with a proximal DPPC (Figure 4) (see Figure 3SC of the Supporting Information). In addition, the serine amino group interacts with another adjacent DPPC through the terminal phosphate oxygens (see Figure 3SD of the Supporting Information). Other interactions consist of a hydrophobic interaction between the glycerol backbone and Leu6, which replaces the interaction with Phe5 that is lost during the simulation. We think that the changes in the interactions observed during the dynamics are the consequence of the lipid membrane, which is missing in the crystal structure. Clearly, the simulations illustrate the important role of the lipid in determining the full complement of interactions of PT1 with DDPS in the presence of a realistic DPPC lipid membrane. In addition, the simulations reveal that one DPPC lipid approaches a surface cavity surrounded by Gla30, Gla8, and Lys11 of PT1 (*14*), suggesting the presence of another phospholipid headgroup binding site.

Phosphatidylserine Binding to the Gla Domain: Second Binding Site. To check whether the potential second binding site is likely to bind a DPPS lipid, the proximal DPPC was substituted with a DPPS. This initial structure was used to conduct a MD simulation with the same protocol described previously for the (PT1−Ca^{2+}/**1PS**)$_{PC}$ system (see Setup of the Simulations). The entire (PT1−Ca^{2+}/**2PS**)$_{PC}$ system was stable during the 10 ns of the MD simulation with a rmsd of the C_α atoms with respect to the initial structure in the range of 0.5−1.0 Å (see Figure 4SA of the Supporting Information). However, the first binding site (DPPS1 headgroup) showed very small deviations with a rmsd of 0.70 ± 0.16 Å throughout the MD simulation, while the DPPS2 headgroup in the second binding site explored a substantial configurational space as indicated by a rmsd of 4 Å with respect to its initial structure (see Figure 4SB of the Supporting Information). The relaxation of the position of the DPPS2 headgroup in the second binding site suggests reasonably good sampling of the orientations, which may not be strongly dependent on initial conditions.

All the interactions in the first binding site that characterized the (PT1−Ca^{2+}/**1PS**)$_{PC}$ system were maintained during the additional 10 ns of dynamics of the (PT1−Ca^{2+}/**2PS**)$_{PC}$ system. The new DPPS binding site shows three main interactions: (1) the terminal phosphate oxygen, OP3, of the second DPPS interacts with Ca1, (2) the amino serine group forms a salt bridge with the carboxyl oxygen (OE2) of Gla30, and (3) the carboxyl oxygens of the second DPPS form a salt bridge with the Nζ atom of Lys11. The initially intermittent Lys11−DPPS interaction finally settles into a stable salt bridge and is maintained until the end of the 10 ns simulations (see Figure 5S of the Supporting Information). Clearly, two of the three residues that were emphasized by MacDonald et al. (*14*) form the potential second phosphatidylserine headgroup binding site of the PT1−Ca^{2+} protein. Ion Ca1 is coordinated by the carboxyl oxygens of Gla26 (OE2) and Gla30 (OE1), the terminal phosphate oxygen (OP3) of DPPS, and water molecules. One of the acyl chains of DPPS forms a hydrophobic interaction with Val9. The main interactions for the second phosphatidylserine binding site are shown in Figure 5.

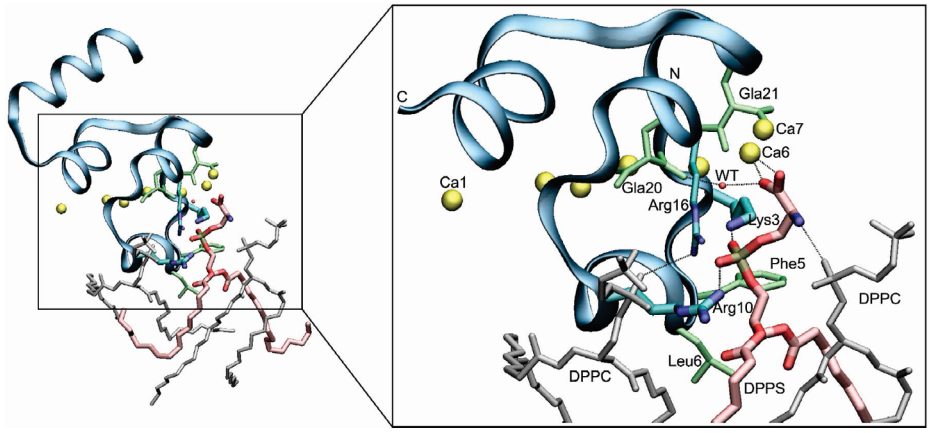

FIGURE 4: Main interactions for the first phosphatidylserine binding site. Hydrogen bonds and salt bridges between atoms of DPPS, the PT1−Ca^{2+} complex, and terminal phosphate oxygens of DPPC. Hydrogen bonds and salt bridges between Arg16 (NH1) and terminal phosphate oxygens of DPPC.

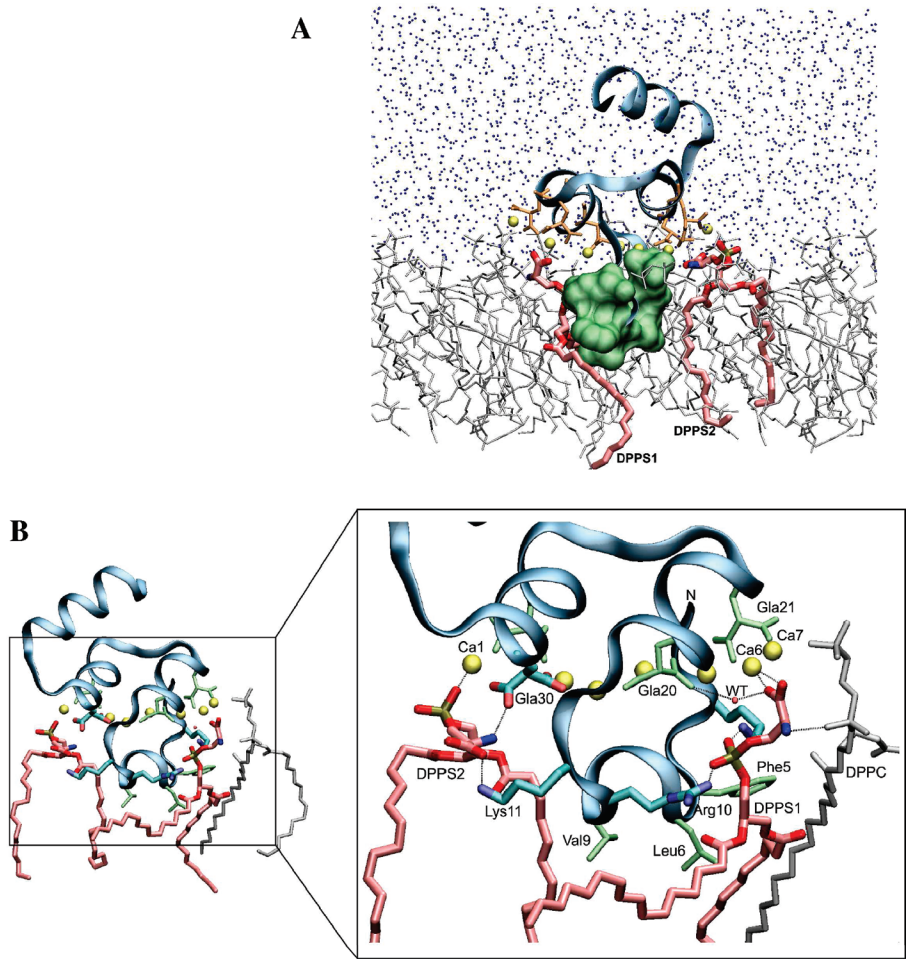

FIGURE 5: Model of the PT1−Ca^{2+} complex interacting with two phosphatidylserines (PS). (A) PT1 is depicted bound to one leaflet of a mixed bilayer compound of phosphatidylcholines (gray) and two PSs (pink). PT1 is shown as ribbons (blue); the Gla residues are colored orange, and the Ca^{2+} ions are colored yellow. The PS1 bound to the first binding site is on the left side, and the PS2 bound to the second binding site is on the right side of the picture. The ω-loop is shown in a solvent accessible surface area model (green), with the Phe5 residue from this loop buried ~7 Å inside the membrane. The water molecules are shown as blue dots. (B) Main interactions for the second phosphatidylserine binding site. Hydrogen bonds and salt bridges between atoms in DPPS and the PT1−Ca^{2+} complex. Panels A and B are rotated 180° with respect to each other to better represent the orientation of the two PS binding sites.

There are clear similarities between the two binding sites, which are characterized by the interaction of the serine carboxylate with Ca^{2+} ions and the interaction of the phosphate group with a positively charged side chain of PT1. However, there are some differences, which are worth noting. The serine amino terminus in the first site interacts with another lipid, whereas in the second site, it interacts with Gla30. Furthermore, there are two positively charged groups (Arg10 and Lys3) in the first site, but only Lys11 is available in the second site. It appears that the second site may bind DPPS less strongly than the first site. The electrostatics potentials in both sites (Figure 6) illustrate the essential

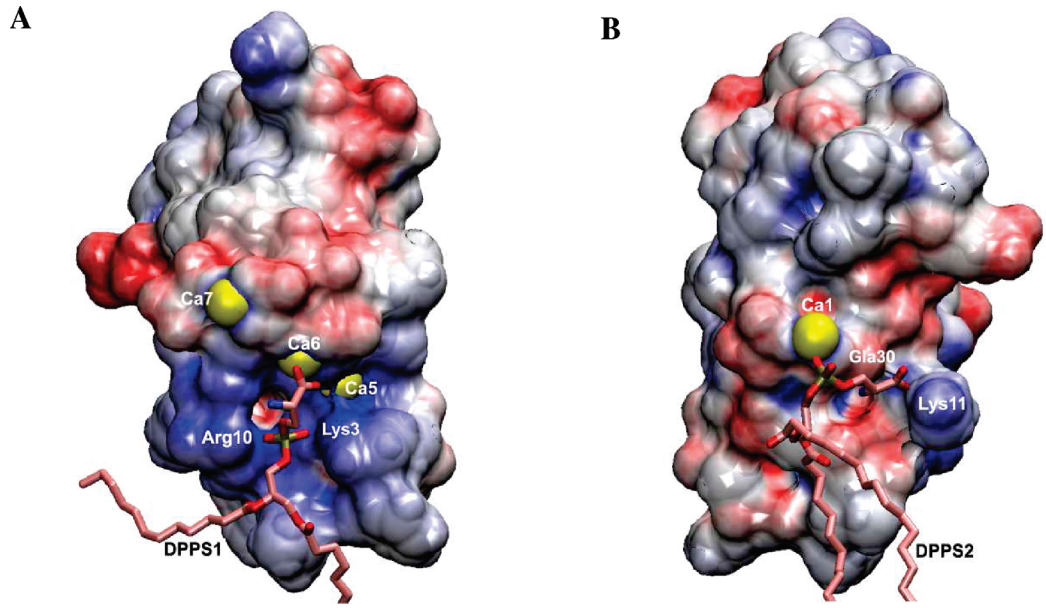

FIGURE 6: Surface electrostatic potential representation of the PT1−Ca^{2+}/**2PS** complex. (A) First phosphatidylserine binding site. (B) Second phosphatidylserine binding site. The electrostatic potential range used in the figures was $\pm 10 k_B T/e$, where k_B, T, and e represent the Boltzmann's constant, the absolute temperature, and the electron charge, respectively. The two phospholipid headgroup binding sites are opposite each other.

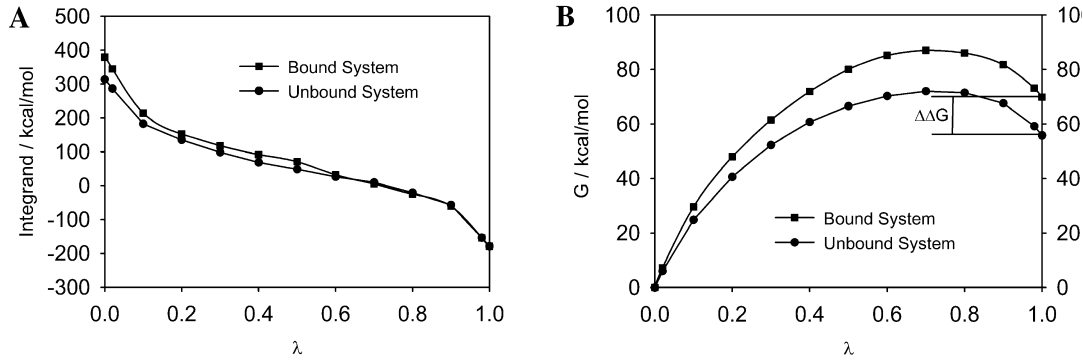

FIGURE 7: Free energy calculations for the first phosphatidylserine binding site. (A) TI integrand for the $(PT1-Ca^{2+}/\mathbf{PS})_{PC} \rightarrow (PT1-Ca^{2+}/\mathbf{PC})_{PC}$ transition. First phosphatidylserine binding site. Eleven points ($\lambda = 0.02$, 0.1−0.9, and 0.98) were used to calculate the free energy differences. The values at the end points were obtained by extrapolation (see the text): run 1 (■, bound system) and run 2 (●, unbound system). (B) Free energy differences.

difference between them. To explore this hypothesis, we conducted free energy perturbation simulations to evaluate the relative free energy of binding of DPPS to PT1 at each of the putative binding sites.

Free Energy Simulations: First Phosphatidylserine Binding Site. To assess the difference in the strength of binding of PT1 to a pure DPPC membrane and to a mixed membrane with one DPPS, we conducted four different free energy simulations. In two simulations, we convert PS → PC^F and PC → PS^B in the presence of PT1 [$\Delta G^{Bound}_{PS \rightarrow PC^F}(PC \rightarrow PS^B)$], and in the other two, the conversion is done in the absence of the protein [$\Delta G^{Unbound}_{PS \rightarrow PC^F}(PC \rightarrow PS^B)$]. The values of the free energy derivatives with respect to λ are depicted in Figure 7A, and the cumulative free energy changes for the bound [$\Delta G^{Bound}_{PS \rightarrow PC^F}(PC \rightarrow PS^B)$] and unbound [$\Delta G^{Unbound}_{PS \rightarrow PC^F}(PC \rightarrow PS^B)$] systems as a function of λ for run 1 are shown in Figure 7B. The potential energy derivatives, $\partial U(\mathbf{r};\lambda)/\partial\lambda$, for each λ in run 1 (PS → PC^F for the unbound and bound systems) as a function of simulation time (Figure S6A,B of the Supporting Information) show that after the equilibration of 50 ps, the energy relaxes to the new λ value and is stabilized at the appropriate value of the integrand. Similar behavior was observed in run 2.

The free energy difference resulting from the different schemes of TI and FEP varies between 14.5 and 13.0 kcal/mol for run 1 and between −8.9 and −9.4 kcal/mol for run 2, which is a reverse mapping. These two mean value extremes correspond to Scheme 3 of the TI and of the FEP, respectively. The mean value of the total free energy difference obtained from FEP is also included in the interval of TI, i.e., $-11.7 \text{ kcal/mol} \leq \overline{\Delta\Delta G} \leq -11.2 \text{ kcal/mol}$. The end point contribution to the free energy is small for all runs (see Table S1 of the Supporting Information for end point contributions to the free energy difference at $\lambda = 0 \rightarrow 0.02$ and $\lambda = 0.98 \rightarrow 1.0$). The results are summarized in Table 4 (see also Table S1 of the Supporting Information).

Runs 1 and 2 represent independent free energy evaluations in the forward PS → PC^F and backward PC → PS^B directions for the bound and unbound systems. The TI and the FEP methods yield essentially the same results; they show that the binding of the PT1−Ca^{2+} complex to the mixed membrane that contains one PS is favorable compared to the binding to a membrane that contains only PC (Table 4 and Table S1). There is clear hysteresis between run 1 and run 2, which amounts to ∼5 kcal/mol. We estimate that

Table 4: Free Energy Differences of PS → PC (and vice versa) in the Absence and Presence of Protein ($PT1-Ca^{2+}$) in a DPPC Lipid Membrane Using FEP and TI[a]

run[b]		ΔG (kcal/mol) TI (Scheme 1)	ΔG (kcal/mol) FEP
1 (PS → PC)	unbound	55.8	56.0
	bound	69.8	69.1
	$\Delta\Delta G^{Binding}$	**14.0**	**13.1**
2 (PC → PS)	unbound	−46.5	−45.7
	bound	−55.5	−55.1
	$\Delta\Delta G^{Binding}$ [c]	**−9.0**	**−9.4**
	$\overline{\Delta\Delta G^{Binding}}$ (SD)[c]	**−11.5 (3.5)**	**−11.3 (2.6)**

[a] First phosphatidylserine binding site. [b] Runs 1 and 2 correspond to the calculation of the free energy of the alchemical interconversion between one PS and one PC in the absence and presence of protein ($PT1-Ca^{2+}$) in a DPPC lipid membrane and vice versa, respectively. [c] $\Delta\Delta G^{Binding}$ is the free energy difference between the bound and unbound systems, and SD is the standard deviation.

Table 5: Free Energy Differences of PS → PC (and vice versa) in the Absence and Presence of Protein ($PT1-Ca^{2+}$) in a DPPC Lipid Membrane Using FEP and TI[a]

run[b]		ΔG (kcal/mol) TI (Scheme 1)	ΔG (kcal/mol) FEP
1 (PS → PC)	unbound	55.8	56.0
	bound	67.3	65.4
	$\Delta\Delta G^{Binding}$	**11.5**	**9.4**
2 (PC → PS)	unbound	−46.5	−45.7
	bound	−53.3	−53.2
	$\Delta\Delta G^{Binding}$ [c]	**−6.8**	**−7.5**
	$\overline{\Delta\Delta G^{Binding}}$ (SD)[c]	**−9.1 (3.3)**	**−8.5 (1.3)**

[a] Second phosphatidylserine binding site. [b] Runs 1 and 2 correspond to the calculation of the free energy of the alchemical interconversion between one PS and one PC in the absence and presence of protein ($PT1-Ca^{2+}$) in a DPPC lipid membrane and vice versa, respectively. [c] $\Delta\Delta G^{Binding}$ is the free energy difference between the bound and unbound systems, and SD is the standard deviation.

configurational contributions from changes in binding of the $PT1-Ca^{2+}$ complex to the different membranes are small with the main contribution to the hysteresis coming from the electrostatic term due to the formation and/or elimination of a charge along the perturbation scheme. In the PS → PC^F simulation, the negative charge of PS is eliminated when it is converted to PC, while in the opposite direction, PC → PS^B, the charge is created. The free energy of eliminating the charge makes a positive contribution to the energy and vice versa. Considering that the hysteresis due to configurational changes is minor, the cost of the electrostatic free energy is relatively small compared to the total difference in the free energy of binding. Assuming that the binding of the $PT1-Ca^{2+}$ complex to the pure PC membrane is negligible, we can consider $\Delta\Delta G$ the free energy of binding to a membrane with only one PS. This is in very good agreement with experimental results that estimate the binding energy to be −9.6 kcal/mol (*14*).

Free Energy Simulations: Second Phosphatidylserine Binding Site. The approach of a DPPC to the suggested second binding site on the $PT1-Ca^{2+}$ site during MD simulations offered an opportunity to explore the importance of such a site in anchoring the protein to the membrane. In addition to equilibrating the position of DPPS in the second binding site (see above), we also estimated the relative binding free energy of the second site in the presence of a DPPS in the first site. Such a calculation is consistent with the experimental structure that shows the binding of DPPS in the first binding site and with experimental suggestions that a potential second binding site exists (*14*). The binding to the second site presents an additional consideration that did not play an important role in the first set of simulations. The binding of the $PT1-Ca^{2+}$ complex to a single DPPS in a DPPC membrane can be treated as a simple association process. However, the binding of an additional DPPS to PT1 requires a relocation of the DPPS in the membrane to the site of binding. Thus, the demixing entropy will have to be considered in the final evaluation of the relative free energy of binding. We divide the evaluation of the free energy into two steps. In the first, we evaluate the free energy using the perturbation from PC headgroup to PS using the same protocol that was used for the calculation of the free energy difference for the first phospholipid binding site. In the second stage, we estimate the entropy associated with the localization of the second DPPS near the binding site.

The values of the free energy difference for both FEP and TI are summarized in Table 5 (see also Table S2 of the Supporting Information). The values of the free energy derivatives with respect to λ are depicted in Figure 8A. The convergence of the calculations shows similar characteristics as in the simulations at site 1. Although there are some fluctuations in the energy at the equilibration period, the system relaxes to the new λ value and is stabilized at the appropriate value of the integrand. As discussed above, runs 1 and 2 represent independent free energy evaluations in the forward PS → PC^F and backward PC → PS^B directions for the bound and unbound systems. They show a similar hysteresis as in the simulations at the first site, and we think they originate from a similar imbalance in the electrostatic term. The PS → PC^F step creates an unbalanced positive charge, which results in an overestimated free energy change, whereas the PC → PS^B step underestimates this term because of the neutralization of the additional charge. As in site 1 simulations, here too the difference between runs 1 and 2 amounts to approximately 5 kcal/mol.

The cumulative free energy changes for the bound $[\Delta G^{Bound}_{PS\rightarrow PC^F}(PC\rightarrow PS^B)]$ and unbound $[\Delta G^{Unbound}_{PS\rightarrow PC^F}(PC\rightarrow PS^B)]$ systems as a function of λ for run 1 are shown in Figure 8B. The free energy resulting from the different schemes of TI and FEP varies between 11.6 and 9.4 kcal/mol for run 1 and between −6.6 and −7.5 kcal/mol for run 2. These two mean value extremes, as in the first binding site, correspond to Scheme 3 of the TI method and FEP method, respectively. The mean value of the total free energy difference obtained from FEP is also included in the interval where the values of the free energy using TI are found, that is, $-9.1 \text{ kcal/mol} \leq \Delta G \leq -8.5$ kcal/mol. The end point contributions to the free energy difference at $\lambda = 0 \rightarrow 0.02$ and $\lambda = 0.98 \rightarrow 1.0$ are small (see Table S2). The potential energy derivatives, $\partial U(\mathbf{r},\lambda)/\partial\lambda$, for each λ in run 1 (PS → PC^F for the unbound and bound systems) as a function of simulation time behave in a manner similar to that described above (see Figure S7 of the Supporting Information).

A comparison of the results in Tables 4 and 5 clearly shows that the free energy of binding in the second site is lower by approximately 2.3 kcal/mol than in the first site. This result is consistent regardless of the particular comparison of the energies, i.e., whether we compare the individual runs in the two systems or the average energy of runs 1 and 2. Clearly, the origin of this difference is in the

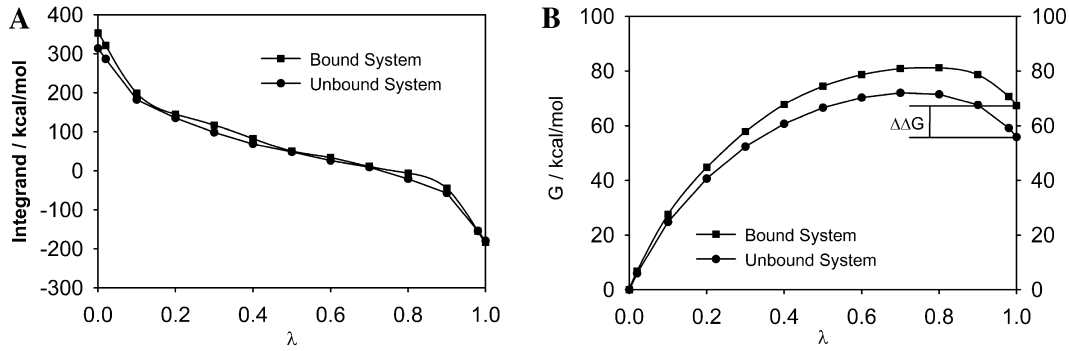

FIGURE 8: Free energy calculations for the second phosphatidylserine binding site. (A) TI integrand for the (PT1−Ca^{2+}/**PS**)$_{PC}$ → (PT1−Ca^{2+}/**PC**)$_{PC}$ transition. Second phosphatidylserine binding site. Eleven points (λ = 0.02, 0.1−0.9, and 0.98) were used to calculate the free energy differences. The values at the end points were obtained by extrapolation (see the text): run 1 (■, bound system) and run 2 (●, unbound system). (B) Free energy differences.

different set of interactions between the PS headgroup and the binding sites (see Phosphatidylserine Binding to the Gla Domain: First Binding Site or Phosphatidylserine Binding to the Gla Domain: Second Binding Site). Since the main change was characterized by a different set of electrostatic interactions, we decomposed the free energy change into the electrostatic and van der Waals components. While such decomposition may be path-dependent, in our particular system the similarity of the simulations suggests that the decomposition may provide an explanation of the origin of the difference between binding to the two sites. Almost all the change in the free energy between sites 1 and 2 comes from a change in the electrostatic energy (∼4.8 kcal/mol), and a smaller fraction with an opposite sign comes from van der Waals interactions and internal energy.

The recruitment of another DPPS to interact with the PT1−Ca^{2+} complex is clearly driven by electrostatic interactions, which provides the necessary entropic cost due to lipid demixing and charge conservation. As demonstrated by May et al. (*40*), the entropic cost due to these effects can be computed from the following equation:

$$\Delta S = -k_B N\left[\varphi_f \ln \frac{\varphi_f}{\varphi_i} + (1-\varphi_f)\ln \frac{1-\varphi_f}{1-\varphi_i}\right] \qquad (6)$$

where k_B is Boltzmann's constant, N is the total number of lipids in the system, and ϕ_f and ϕ_i are the final and initial density of the DPPS, respectively. Considering that we start with one DPPS out of 22 lipids and increase the number to two, we estimate the entropic cost to be 0.82 entropy unit, which results in a free energy increase of ∼0.3 kcal/mol. Thus, the final estimate of the binding free energy of DPPS in the second site of the PT1−Ca^{2+} complex is −8.8 kcal/mol, almost 3 kcal/mol lower than in site 1. This weaker binding may be related to the fact that it has been difficult to observe it in crystallographic studies.

CONCLUSIONS

We have simulated the PT1−Ca^{2+} system with one and two DPPSs in a DPPC bilayer membrane with the aim of investigating the molecular basis for binding of the Gla domain to phosphatidylserine-containing membranes. Specifically, we tried to predict the existence of a second phosphatidylserine binding site, which was suggested to consist of Gla30, Gla8, and Lys11 that form a surface cavity (*14*).

The well-defined phosphatidylserine binding site characterized in the crystal structure of PT1−Ca^{2+} protein in complex with lysoPS (*5*) is maintained in our simulations. However, some of the interactions change in the course of the simulation. For example, the interaction of Arg16 with the terminal phosphate of DPPS as well as the acyl chain of DPPS with Phe5 of the ω-loop is replaced with the equivalent groups of a proximal DPPC. This could be related to the presence of the lipid membrane, which is missing in the crystal structure. Our results also predict the existence of a second phospholipid headgroup binding site on the opposite face with respect to the well-defined phosphatidylserine binding site. This is in general agreement with a site proposed by MacDonald et al. (*14*).

From the FEP calculations, we can estimate the energy of binding of the PT1−Ca^{2+} complex to DPPS to be around −11.5 kcal/mol. Most of the binding energy comes from electrostatic interactions between the positively charged protein and the negative phospholipids. Site 2 clearly shows fewer potential electrostatic interactions, which results in a lower binding energy. Since the binding of a second DPPS requires a rearrangement of the charged lipids, the entropic cost associated with this is on the order of 0.3 kcal/mol. Taken together, the binding free energy for the second site is estimated to be around −8.8 kcal/mol.

Considering that most of the interactions between PT1 and the lipid involve highly charged Ca^{2+} ions and polarizable phospholipid headgroups, it seems relevant to mention that polarization effects have not been included in the FEP calculations presented here. Considerable effort has been invested in recent years to reparametrize the force fields to include a polarization effect, but the effect of such a term on the thermodynamics and on sampling is not yet available. A recent review (*41*) predicts the usefulness of such force fields in simulations while noting that such an approach breaks the assumption of simple additivity. There is clear evidence (*42*) that polarization affects the dynamics and distribution of configurational properties, but the effect on thermodynamic properties is currently not well documented.

Anchoring blood-borne proteins important in blood coagulation to cell membranes in the vicinity of blood vessel damage is of major importance. It not only localizes these essential proteins to the point of damage but also enhances the catalytic activity of the enzymes that are anchored to a surface by increasing their effective concentration. The regulation of the anchoring to the negatively charged

phosphatidylserines on the outer leaf of the cell is controlled by the electrostatic interactions and by the entropic effects of localizing the lipids in the vicinity of the protein. We show here that the interactions with the lipid are quite substantial and that the entropic cost is rather small. Prothrombin has two potential sites for such an interaction. While the contributions from each of the sites are different, they effectively anchor prothrombin by electrostatic interactions. Other Gla-containing proteins may be anchored in a similar way, enhancing the catalytic events essential for blood coagulation.

ACKNOWLEDGMENT

Y.R. dedicates this manuscript to the memory of his father, Jacinto.

SUPPORTING INFORMATION AVAILABLE

Local dual topology of the PS/PC hybrid residue (Figure S1), rmsd as a function of time (Figures S2 and S4), distances of different reference atoms as a function of time (Figures S3 and S5), TI integrand as a function of time (Figures S6 and S7), and free energy differences (Tables S1 and S2). This material is available free of charge via the Internet at http://pubs.acs.org.

REFERENCES

1. Jesty, J., and Nemerson, Y. (1995)The pathways of blood coagulation. In *Williams Hematology* (Beutler, E., Lichtman, M. A., Coller, B. S., and Kipps, T. J., Eds.) 5th ed., pp 1227−1238, MacGraw-Hill, New York.
2. Lentz, B. R. (2003) Exposure of platelet membrane phosphatidylserine regulates blood coagulation. *Prog. Lipid Res. 42*, 423–438.
3. Furie, B., and Furie, B. C. (1990) Molecular basis of vitamin K-dependent γ-carboxylation. *Blood 75*, 1753–1762.
4. Rosing, J., Tans, G., Goversriemslag, J. W. P., Zwaal, R. F. A., and Hemker, H. C. (1980) Role of phospholipids and factor-Va in the prothrombinase complex. *J. Biol. Chem. 255*, 274–283.
5. Huang, M., Rigby, A. C., Morelli, X., Grant, M. A., Huang, G., Furie, B., Seaton, B., and Furie, B. C. (2003) Structural basis of membrane binding by Gla domains of vitamin K-dependent proteins. *Nat. Struct. Biol. 10*, 751–756.
6. Kulman, J. D., Harris, J. E., Xie, L., and Davie, E. W. (2001) Identification of two novel transmembrane γ-carboxyglutamic acid proteins expressed broadly in fetal and adult tissues. *Proc. Natl. Acad. Sci. U.S.A. 98*, 1370–1375.
7. Luo, G. B., Ducy, P., McKee, M. D., Pinero, G. J., Loyer, E., Behringer, R. R., and Karsenty, G. (1997) Spontaneous calcification of arteries and cartilage in mice lacking matrix GLA protein. *Nature 386*, 78–81.
8. Zhai, X., Srivastava, A., Drummond, D. C., Daleke, D., and Lentz, B. R. (2002) Phosphatidylserine binding alters the conformation and specifically enhances the cofactor activity of bovine factor Va. *Biochemistry 41*, 5675–5684.
9. Koppaka, V., Wang, J. F., Banerjee, M., and Lentz, B. R. (1996) Soluble phospholipids enhance factor X(a)-catalyzed prothrombin activation in solution. *Biochemistry 35*, 7482–7491.
10. Srivastava, A., Wang, J. F., Majumder, R., Rezaie, A. R., Stenflo, J., Esmon, C. T., and Lentz, B. R. (2002) Localization of phosphatidylserine binding sites to structural domains of factor X-a. *J. Biol. Chem. 277*, 1855–1863.
11. Mizuno, H., Fujimoto, Z., Atoda, H., and Morita, T. (2001) Crystal structure of an anticoagulant protein in complex with the Gla domain of factor X. *Proc. Natl. Acad. Sci. U.S.A. 98*, 7230–7234.
12. Soriano-Garcia, M., Padmanabhan, K., de Vos, A. M., and Tulinsky, A. (1992) The Ca^{2+} ion and membrane binding structure of the Gla domain of Ca-prothrombin fragment 1. *Biochemistry 31*, 2554–2566.
13. Falls, L. A., Furie, B. C., Jacobs, M., Furie, B., and Rigby, A. C. (2001) The ω-loop region of the human prothrombin γ-carboxyglutamic acid domain penetrates anionic phospholipid membranes. *J. Biol. Chem. 276*, 23895–23902.
14. McDonald, J. F., Shah, A. M., Schwalbe, R. A., Kisiel, W., Dahlback, B., and Nelsestuen, G. L. (1997) Comparison of naturally occurring vitamin K-dependent proteins: Correlation of amino acid sequences and membrane binding properties suggests a membrane contact site. *Biochemistry 36*, 5120–5127.
15. Roux, B. Building a configuration for a membrane/protein system. http://thallium.bsd.uchicago.edu/RouxLab/method.html.
16. De Loof, H., Harvey, S. C., Segrest, J. P., and Pastor, R. W. (1991) Mean Field Stochastic Boundary Molecular-Dynamics Simulation of a Phospholipid in a Membrane. *Biochemistry 30*, 2099–2113.
17. Pastor, R. W., Venable, R. M., and Karplus, M. (1991) Model for the structure of the lipid bilayer. *Proc. Natl. Acad. Sci. U.S.A. 88*, 892–896.
18. Venable, R. M., Zhang, Y., Hardy, B. J., and Pastor, R. W. (1993) Molecular dynamics simulations of a lipid bilayer and of hexadecane: An investigation of membrane fluidity. *Science 262*, 223–226.
19. Rodríguez, Y., Mezei, M., and Osman, R. (2006) Association free energy of dipalmitoylphosphatidylserines in a mixed dipalmitoylphosphatidylcholine membrane. *Biophys. J. 92*, 3071–3080.
20. Jedlovszky, P., and Mezei, M. (1999) Grand canonical ensemble Monte Carlo simulation of a lipid bilayer using extension biased rotations. *J. Chem. Phys. 111*, 10770–10773.
21. Feller, S. E., and MacKerell, A. D. (2000) An improved empirical potential energy function for molecular simulations of phospholipids. *J. Phys. Chem. B 104*, 7510–7515.
22. Jorgensen, W. L., Chandrasekhar, J., Madura, J. D., Impey, R. W., and Klein, M. L. (1983) Comparison of simple potential functions for simulating liquid water. *J. Chem. Phys. 79*, 926–935.
23. Ryckaert, J. P., Ciccotti, G., and Berendsen, H. J. C. (1977) Numerical integration of cartesian equations of motion of a system with constraints molecular dynamics of n-alkanes. *J. Comput. Phys. 23*, 327–341.
24. Brooks, B. R., Bruccoleri, R. E., Olafson, B. D., States, D. J., Swaminathan, S., and Karplus, M. (1983) CHARMM: A program for macromolecular energy, minimization, and dynamics calculations. *J. Comput. Chem. 4*, 187–217.
25. Phillips, J. C., Braun, R., Wang, W., Gumbart, J., Tajkhorshid, E., Villa, E., Chipot, C., Skeel, R. D., Kale, L., and Schulten, K. (2005) Scalable molecular dynamics with NAMD. *J. Comput. Chem. 26*, 1781–1802.
26. Essmann, U., Perera, L., Berkowitz, M. L., Darden, T., Lee, H., and Pedersen, L. G. (1995) A smooth particle mesh Ewald method. *J. Chem. Phys. 103*, 8577–8593.
27. Darden, T., York, D., and Pedersen, L. (1993) Particle mesh Ewald: An N.Log(N) method for Ewald sums in large systems. *J. Chem. Phys. 98*, 10089–10092.
28. Pearlman, D. A. (1994) A comparison of alternative approaches to free-energy calculations. *J. Phys. Chem. 98*, 1487–1493.
29. Mezei, M., and Beveridge, D. L. (1986) Free energy simulations. *Ann. N.Y. Acad. Sci. 482*, 1–23.
30. Resat, H., and Mezei, M. (1993) Studies on Free-Energy Calculations. 1. Thermodynamic Integration Using a Polynomial Path. *J. Chem. Phys. 99*, 6052–6061.
31. Boresch, S., and Karplus, M. (1999) The role of bonded terms in free energy simulations: 1. Theoretical analysis. *J. Phys. Chem. A 103*, 103–118.
32. Boresch, S., and Karplus, M. (1999) The role of bonded terms in free energy simulations. 2. Calculation of their influence on free energy differences of solvation. *J. Phys. Chem. A 103*, 119–136.
33. Tidor, B., and Karplus, M. (1991) Simulation analysis of the stability mutant R96H of T4 lysozyme. *Biochemistry 30*, 3217–3228.
34. Simonson, T., Archontis, G., and Karplus, M. (1997) Continuum treatment of long-range interactions in free energy calculations. Application to protein-ligand binding. *J. Phys. Chem. B 101*, 8349–8362.
35. Michielin, O., and Karplus, M. (2002) Binding free energy differences in a TCR-peptide-MHC complex induced by a peptide mutation: A simulation analysis. *J. Mol. Biol. 324*, 547–569.
36. Zeng, J., Fridman, M., Maruta, H., Treutlein, H. R., and Simonson, T. (1999) Protein-protein recognition: An experimental and computational study of the R89K mutation in Raf and its effect on Ras binding. *Protein Sci. 8*, 50–64.

37. Archontis, G., Simonson, T., Moras, D., and Karplus, M. (1998) Specific amino acid recognition by aspartyl-tRNA synthetase studied by free energy simulations. *J. Mol. Biol. 275*, 823 846.
38. White, S. H., and Wiener, M. C. (1996)The liquid-crystallographic structure of fluid lipid bilayer membranes. In *Biological Membranes: A Molecular Perspective from Computation and Experiment* (Merz, K. M., and Roux, B., Eds.) pp 127−144, Birkhäuser, Boston.
39. Mezei, M. (2008)MMC: Monte Carlo program for simulation of molecular assemblies. http://inka.mssm.edu/∼mezei/mmc.
40. May, S., Harries, D., and Ben-Shaul, A. (2000) Lipid demixing and protein-protein interactions in the adsorption of charged proteins on mixed membranes. *Biophys. J. 79*, 1747–1760.
41. Boas, F. E., and Harbury, P. B. (2007) Potential energy functions for protein design. *Curr. Opin. Struct. Biol. 17*, 199–204.
42. Ji, C., Mei, Y., and Zhang, J. Z. (2008) Developing polarized protein-specific charges for protein dynamics: MD free energy calculation of pKa shifts for Asp26/Asp20 in thioredoxin. *Biophys. J. 95*, 1080–1088.

BI801199V